Levitation of fizzy drops

As Published: 10.1126/sciadv.abf0888

Publisher: American Association for the Advancement of Science (AAAS)

Persistent URL: https://hdl.handle.net/1721.1/133254

Version: Final published version: final published article, as it appeared in a journal, conference proceedings, or other formally published context

APPLIED SCIENCES AND ENGINEERING

Levitation of fizzy drops

Divya Panchanathan†, Philippe Bourrianne†, Philippe Nicollier, Abhijatmedhi Chottratanapituk, Kripa K. Varanasi*, Gareth H. McKinley*

As first described by Leidenfrost, liquid droplets levitate over their own vapor when placed on a sufficiently hot substrate. The Leidenfrost effect not only confers remarkable properties such as mechanical and thermal insulation, zero adhesion, and extreme mobility but also requires a high energetic thermal cost. We describe here a previously unexplored approach using active liquids able to sustain levitation in the absence of any external forcing at ambient temperature. We focus on the particular case of carbonated water placed on a superhydrophobic solid and demonstrate how millimetric fizzy drops self-generate a gas cushion that provides levitation on time scales on the order of a minute. Last, we generalize this new regime to different kinds of chemically reactive droplets able to jump from the Cassie-Baxter state to a levitating regime, paving the way to the levitation of non-volatile liquids.

INTRODUCTION

Liquid droplets can be levitated using various external forcing such as vibrations (*1*), air flows (*2*), acoustic waves (*3*), magnetic forces (*4*), or even their own evaporation (*5*, *6*). A volatile liquid indeed levitates on its vapor when deposited on a very hot solid, as initially described by Leidenfrost (*5*). The absence of liquid-solid contact provides Leidenfrost droplets with intriguing properties such as zero adhesion, drag reduction (*7*, *8*), extreme mobility (*9*–*12*), and thermal insulation (*6*, *13*). However, the prerequisite high substrate temperature (*14*) limits the industrial application of Leidenfrost effects, and efforts have been made to lower the Leidenfrost temperature down to the boiling point of water (*15*–*17*). Here, we report a novel approach using supersaturated liquids to enable droplet levitation in the absence of any external forcing. We describe how carbonated water droplets deposited on a water-repellent solid can be levitated for time scales on the order of a minute at ambient temperature. Levitation occurs above a critical CO_2 concentration, an analog of the Leidenfrost temperature. This new regime of levitation exhibits similar properties to Leidenfrost drops in terms of levitation time, antiadhesion, extremely low friction, and even self-propulsion. However, this phenomenon enables drop levitation without requiring a specific criterion of liquid volatility. Last, we extend this concept to other gas-generating techniques based on chemically active liquids able to jump from a Cassie-Baxter wetting state to a levitating regime.

Water drops are known to be strongly repelled by superhydrophobic substrates, combining both hydrophobic chemistry and micrometric roughness (*18*). As seen in Fig. 1A, a drop deposited on a silicon wafer made superhydrophobic by a commercially available coating (later denoted as Glaco; see Materials and Methods and section S1) adopts a quasi-spherical shape and shows very high values of contact angles, as evidenced in the magnified view in Fig. 1C. In this so-called Cassie-Baxter state (*18*), the water drop sits on the tops of the hydrophobic texture (Fig. 1B), leading to a solid-liquid contact area that is reduced to a tiny fraction of its basal area. In Fig. 1D, we also observe the bottom area of a drop deposited on a transparent Glaco-coated glass substrate with an interferomicroscopy setup (see Materials and Methods and section S11). Here, the combination of dark and bright spots in Fig. 1D is the hallmark of heterogeneous wetting in the Cassie-Baxter state. However, this low-adhesion regime is metastable in many circumstances (*19*), and an external perturbation eventually leads to another regime (the Wenzel state) in which the liquid invades the hydrophobic porosity of the textured substrate, causing a marked increase in adhesion (*19*–*21*). Providing a lift force to promote levitation of the droplet on our substrate at ambient temperature can prevent such transitions by eliminating any local contact between the solid and the liquid drop.

Department of Mechanical Engineering, Massachusetts Institute of Technology, 77 Massachusetts Avenue, Cambridge, MA 02139, USA.
*Corresponding author. Email: gareth@mit.edu (G.H.M.); varanasi@mit.edu (K.K.V.)
†These authors contributed equally to this work.

RESULTS AND DISCUSSION

Fizzy levitation

In this work, we propose a novel method to levitate water droplets using superhydrophobic coatings and active liquids that are able to sustain their own levitation in the absence of external stimulus. We particularly describe the case of "fizzy" water droplets that are supersaturated with dissolved gas. Here, we use the excess chemical energy stored inside the droplet in the form of dissolved gas to drive levitation instead of relying on external energy sources such as heat or mechanical motion. The chemical potential difference between the dissolved gas in the drop and the residual presence of the gas in the surrounding phase drives a mass flux from the liquid into the environment, analogous to the evaporative flux driven by a temperature difference in the Leidenfrost regime. We prepare carbonated water by pressurizing gaseous carbon dioxide into deionized (DI) water. We tune the initial CO_2 concentration C_0 by controlling the pressurization and quantify it through pH measurements (section S2). When a carbonated water drop of initial concentration $C_0 \approx 168$ mM is deposited on the Glaco-coated wafer and held in place by a needle (Fig. 1E), a quasi-spherical shape is observed, equivalent to the still (uncarbonated) water in Fig. 1A. However, we can observe light passing between the drop and its reflection on the substrate similar to the original observations of Leidenfrost (movie S1) (*5*, *6*). As shown in the magnified picture in Fig. 1G, we detect an air gap between the drop and the superhydrophobic wafer. This thin gap of thickness $h \approx 3$ μm is a signature of the levitating droplet regime sketched in Fig. 1F. The released CO_2 is temporarily trapped

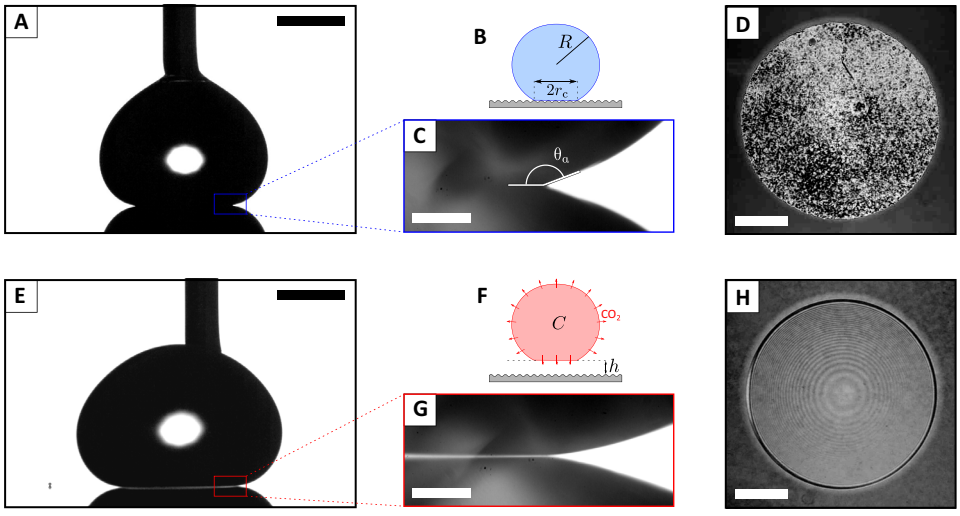

Fig. 1. From the Cassie-Baxter state to drop levitation. (**A**) Photograph of a 40-μl water drop held by a needle on a superhydrophobic wafer. Scale bar, 2 mm. (**B**) Sketch (not to scale) of a millimeter-sized drop (radius R and contact radius r_c) of water in the Cassie-Baxter state. (**C**) Zoomed picture of the bottom edge of a 40-μl drop in the Cassie-Baxter state with an apparent contact angle $\theta_a = 167°$. Scale bar, 100 μm. (**D**) Bottom view of a 40-μl deionized (DI) water drop deposited on a transparent Glaco-coated glass slide using interferomicroscopy. Scale bar, 500 μm. (**E**) Picture of a 60-μl carbonated water drop ($C_0 \approx 168$ mM) held by a needle on a Glaco-coated wafer. A thin ray of light is noticeable between the drop and its reflection. Scale bar, 2 mm. (**F**) Sketch (not to scale) of a millimeter-sized drop of carbonated water releasing CO_2 and levitating over a thin cushion of gas of thickness h. (**G**) Magnified view of the bottom edge of a 40-μl carbonated water drop ($C_0 \approx 168$ mM). A thin gap ($h \approx 3$ μm) appears between the liquid and its reflection on the solid, demonstrating levitation. Scale bar, 100 μm. (**H**) Bottom view of a 40-μl carbonated water drop deposited on a Glaco-coated glass slide. Interference fringes indicate complete levitation as reported in the classical Leidenfrost regime (*12*, *22*). Scale bar, 500 μm.

underneath the drop and insulates the liquid from contacting the underlying superhydrophobic substrate. As seen in Fig. 1H, the droplet base is still circular when viewed from below but now exhibits its interference fringes, a signature of levitation (*22*). Optical interference due to the thin gap between the top surface of the textured solid and the flattened liquid-gas interface underneath the drop produces Newton's rings comparable to the ones observed in the Leidenfrost regime (*12*, *22*). Our carbonated water drops thus levitate spontaneously at ambient temperature. Such levitation is in obvious contradiction with the usual observations of fizzy beverages in contact with a glass or a plastic bottle and requires a strongly water-repellent (i.e., superhydrophobic) substrate, as discussed in section S13.

However, just similar to how Leidenfrost drops vanish after a few minutes, levitation of carbonated water drops is not permanent and can be seen as a transient state on the path toward thermodynamic equilibrium. To study the temporal dependence of carbonated levitation, we observe the interface beneath our drops with an interferomicroscopy setup sketched in Fig. 2A by depositing a 40-μl carbonated water drop of initial $CO_{2(aq)}$ concentration $C_0 = 104 \pm 10$ mM on a transparent superhydrophobic-coated glass slide. The drops are held stationary in the field of view of the microscope by using annular rings that have been treated to make them superhydrophobic (see section S12). After initial deposition (Fig. 2B, i), we detect the interference fringes characterizing levitation (movies S2 and S3). These fringes persist for approximatively 20 s, although their exact pattern evolves with time, indicating changes in both thickness and conformation of the insulating gas layer (Fig. 2B, ii). After a levitation time of $\tau \approx 20$ s, the liquid finally touches the superhydrophobic solid. The first contact happens at the edge of the drop ($r = r_c \approx 0.9$ mm) as evident in Fig. 2B, iii. While the large gas bubble (or blister) remains at the center of the drop base, the liquid-solid contact is weak and confined to the periphery of the droplet, allowing us to define an edge-pinning transition. This contact region lastly spreads slowly inwards (Fig. 2B, iv) until it covers the entire interface (Fig. 2B, v), resulting in a distinct speckle pattern similar to the one shown in Fig. 1D for an uncarbonated water drop in the Cassie-Baxter state on a superhydrophobic solid (movie S3) and sharply contrasting with the levitating regime. We can thus define the wetting time τ^* at which the carbonated water drop enters a regular Cassie-Baxter state (here, $\tau^* \approx 95$ s). Whereas Leidenfrost drops finally vanish because of their complete evaporation, these carbonated water drops persist even after levitation is complete.

To obtain a closer look at the dynamics of levitation, we study the profile of the gas-liquid interface underneath the drop. As reported in the Leidenfrost regime (*12*, *22*) and predicted in the general case of levitating drops (*23*), the underside of these levitating fizzy drops is curved because of the formation of a central dimple (with radius of curvature R_b) that seeks to rise due to buoyancy (Fig. 2A) (*6*). The thickness of the gas layer reaches a minimum value h at the edge of the base ($r = r_c$) and is maximal at the center of the droplet ($z = h + H_b$ at $r = 0$, with H_b as the height of the dimple). At the end of the levitation regime ($t > \tau$), because of the edge-pinning transition, a blister (also defined by H_b and R_b) is observed, as shown in Fig. 2B (iii). Using interferomicroscopy, we image successive fringes as seen in Fig. 2B, allowing us to extract the evolution in the relative height $\delta(r)$ of the interface underneath our drop $\delta(r) = z(r) - h$ (section S4). Moreover, as discussed later, the minimum thickness h can also be estimated (section S5), enabling us to determine the absolute height of the gas-liquid interface $z(r)$. In Fig. 2C, we report the profile $z(r)$ of the drop in the levitating regime ($t < \tau = 20$ s). The symbols represent our measurements, while the solid lines are obtained by fitting the central bubble profile by a

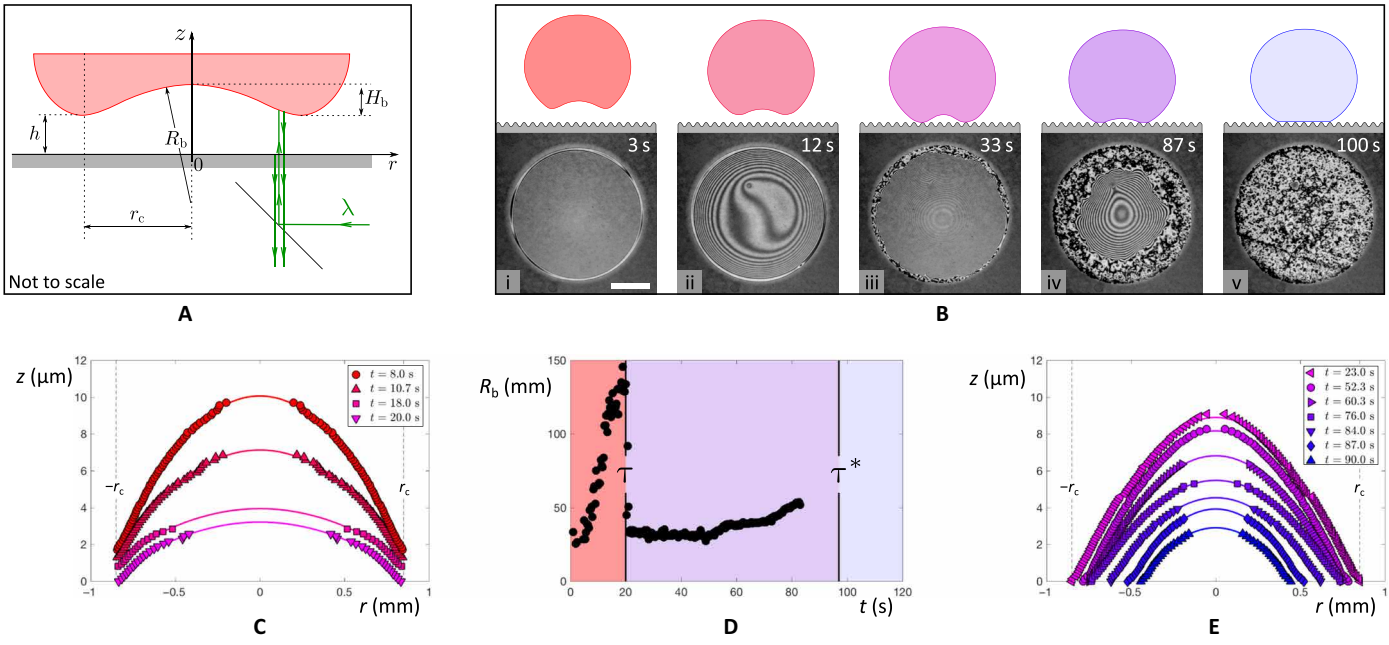

Fig. 2. Lifetime of a carbonated water drop on a superhydrophobic surface. (**A**) Sketch of a levitating drop deposited on a transparent superhydrophobic substrate. Using interferomicroscopy, we measure the height profile $z(r)$ of the gas-liquid interface underneath the drop, its minimum thickness h at the edge ($r = r_c$), and the instantaneous radius of curvature R_b and height H_b of the central bubble. (**B**) Sequence of images of a carbonated water drop base of initial concentration $C_0 = 104$ mM after deposition on a superhydrophobic transparent substrate. As sketched above, the drop first levitates ($t < 20$ s) before experiencing edge pinning ($t = 33$ s), creating a central blister that finally collapses ($t = 87$ s) to reach a Cassie-Baxter state ($t = 100$ s). Scale bar, 0.5 mm. (**C**) Profiles $z(r)$ of the bottom interface of the drop during levitation ($t < 20$ s). A bubble is observed in the center of the drop, its volume decreases over time. (**D**) Evolution of the radius of curvature $R_b(t)$ of the central bubble below the drop after deposition. A sharp transition defines the end ($t = \tau$) of the levitation regime (red). A blister persists afterwards (purple) up to the final touchdown time τ^* when the drop enters the Cassie-Baxter state (blue). (**E**) Profile $z(r)$ of the gas-liquid interface underneath the drop in the blister regime ($t > 20$ s). The bubble height decreases over time. Liquid-solid contacts spread radially inwards from the edges to the center of the droplet base.

quadratic shape, in good agreement with the spherical cap approximation $z \approx h + H_b - r^2/(2R_b)$ with $H_b << R_b$. The profiles in Fig. 2C exhibit a clear evolution from a bubble height of around 8 μm at $t = 8$ s after deposition (red data) to a value reduced by a factor of three after 20 s (pink triangles). Moreover, the quadratic fit gives us an estimation of both geometrical parameters of the bubble (H_b and R_b). The evolution of the two parameters are coupled together and are inversely proportional in the levitating regime when the contact radius r_c of the drop is constant: $H_b \approx r_c^2/(2R_b)$. As predicted for a millimetric-scale drop (*23*), the height H_b of the central bubble is small (on the order of a few microns) compared to r_c. In Fig. 2D, we report the variation in R_b (as estimated by the quadratic fit) with time t. The radius of curvature R_b of the central bubble underneath the dimpled drop is initially ≈25 mm shortly after the drop deposition, which indicates small yet measurable curvature. As time progresses, R_b increases rapidly, leading to a decrease of curvature, i.e., the interface flattens. The gas entrapped underneath the drop drains out of the thin gap. The dimple radius of curvature finally reaches a maximum value of about $R_b \approx 150$ mm at the levitation time $t \rightarrow \tau = 20$ s. At this critical time, R_b experiences a sharp and sudden decrease. In less than a second, the radius of curvature of the central bubble decreases by a factor of four to regain its initial value; this is due to the progressive appearance of contact points between the liquid and the solid at the edge of the drop base ($r = r_c$). This edge-pinning transition leads to a reduction in the number of pathways for the gas exiting the liquid and an increase in pressure within the dimpled vapor bubble. Consequently, the apex height H_b of the bubble rises and the radius of curvature R_b decreases at the end of levitation (section S6). These sharp transitions allow us to precisely define the value of levitation time τ.

The levitating regime (red area in Fig. 2D) is followed by a longer second regime ($\tau < t < \tau^*$) in which a pinned blister is still present below the drop (purple frame in Fig. 2D), allowing partial levitation in which limited contacts between solid substrate and liquid drop exist but are reduced compared to the Cassie-Baxter state. The shape of this bubble can also be measured by interferometry and is plotted in Fig. 2E. The blister height is initially around 10 μm at $t = 23$ s but decreases slowly down to ~3 μm after 90 s. In this partially levitating regime, the gas trapped after touchdown initially accumulates in a bubble whose profile can also be fitted by a quadratic shape. However, over time, the trapped gas eventually flows through the porosity of the superhydrophobic coating, in a similar manner to previous reports on warm superhydrophobic solids in the presence of vapor patches partially covering the drop basal area (*17*). The volume of the blister then decreases slowly and irreversibly, leading to a noticeable decrease in H_b as captured in Fig. 2E. Similarly, the radius of curvature of the bubble (R_b) increases slowly over time during the blister regime indicated in Fig. 2D (purple shading). As liquid-solid contacts spread radially inwards from the edges to the center of the drop base, we reach the Cassie-Baxter state at time τ^* when no gas blister remains. This fizzy levitation process at ambient temperature not only allows us to preserve the volume of the drop at the end of levitation (light blue area, $t > \tau^*$ in Fig. 2D) but also leads to an intermediate regime of lower adhesion ($\tau < t < \tau^*$).

However, the dynamics of the levitation is affected by the concentration C_0 of $CO_{2(aq)}$ initially dissolved in the droplet. By visualizing the drop basal area using the interferomicroscopy setup, we do not observe levitation below a critical concentration of $CO_{2(aq)}$ denoted as C_l, an analog of the critical Leidenfrost temperature T_l. The onset of levitation reported in Fig. 3A appears to be set by a critical $CO_{2(aq)}$ concentration $C_l \approx 7 \pm 3$ mM. Using Henry's law with a constant $k_H = 3.6 \times 10^{-2}$ mM/atm (*24*), this leads to an equivalent partial pressure $P_l = C_l/k_H \approx 0.2$ atm, i.e., somewhat smaller than atmospheric pressure P_0. However, CO_2 is released from carbonated droplets at even smaller initial saturations because the atmospheric partial pressure of CO_2 is typically ~3×10^{-4} atm (*25*). This indicates the necessity to reach high initial levels of gas saturation in our drop to provide levitation, a similar constraint as observed in the Leidenfrost regime, where drop levitation is only triggered in a superheated regime far above the typical evaporative limit (i.e., T_l is always larger than the boiling point of the liquid) (*14*, *15*, *17*).

Below the critical concentration C_l, gas is still released from the saturated drop and eventually leads to a partial levitation (depicted in purple in Fig. 3A). As better seen in the inset pictures of Fig. 3A, the drop base can sustain multiple gas blisters spreading laterally across the superhydrophobic, or "superaerophilic" (*26*), solid. However, these gas patches do not span the entire drop base and fail to provide complete levitation. This partial regime acts as a transitional behavior between a Cassie-Baxter state below $C_p \approx 0.7 \pm 0.3$ mM (blue area in Fig. 3A, where no blisters are detected by our microscopy setup) and levitation above C_l. The fractional gas coverage on the textured superhydrophobic solid grows continuously with the initial concentration of CO_2, similar to recent reports on warm water-repellent solids in which vapor progressively invades the porosity of the hydrophobic textures at temperatures below T_l and even below the boiling point of the liquid droplet (*17*).

In the levitating regime (above C_l), we extract and quantify a levitation time τ from the visualizations of the drop basal area, as discussed in Fig. 2. In Fig. 3A, the levitation time τ is reported as a function of the initial CO_2 concentration C_0 of a carbonated drop of constant volume of 40 μl. Below C_l, in the absence of levitation, $\tau = 0$. Levitation times increase with the amount of CO_2 dissolved in the droplet. We observe levitation times ranging from several seconds up to $\tau \approx 33$ s for higher initial $CO_{2(aq)}$ concentrations. The values of the levitation time are captured by a simple scaling considering a uniform release rate of the $CO_{2(g)}$ across the entire surface area of the carbonated water drop. This slow release rate leads to a regime limited by the diffusion of $CO_{2(g)}$ around the drop (see section S8). The levitation time is set by the initial amount of $CO_{2(g)}$ dissolved inside the droplet and increases monotonically with the initial volume Ω of the drop as $\tau \approx \frac{\Omega^{2/3}}{\alpha^2 D_a}\left(RTk_H\frac{C_0 - C_l}{C_l}\right)^{2/3}\left(\frac{3}{2\pi}\right)^{2/3}$ with D_a as the diffusivity of $CO_{2(g)}$ in the ambient air, k_H as the Henry's law constant, and α as a numerical parameter on the order of unity (see section S8 and the dashed line in Fig. 3A).

The key parameter mediating droplet levitation is the minimum thickness h of the gas layer. By using the interferomicroscopy setup sketched in Fig. 2A, we can measure $h(t)$ during levitation by focusing on the edge of the drop base ($r = \pm r_c$) and counting fringes, while $h(t)$ decreases continuously until touchdown (see section S5 and movie S4). The time dependency of h is discussed in more detail in section S7; here, we focus on the initial thickness h_0 of the gas layer. In Fig. 3B, we report values for h_0 as a function of the initial

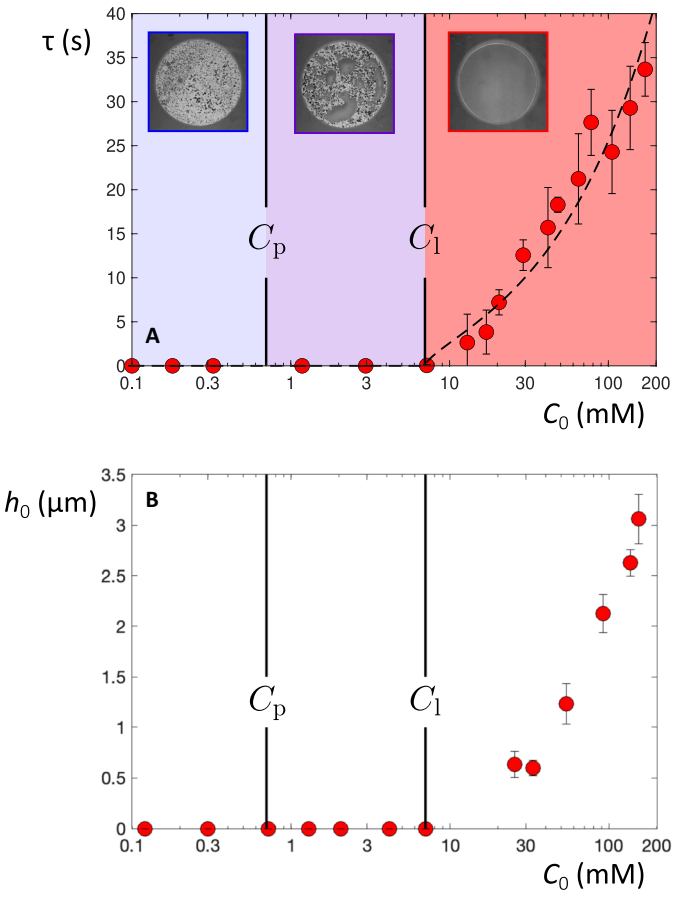

Fig. 3. Characterization of the levitating regime. (**A**) Levitation time τ of a carbonated drop as a function of the initial concentration C_0. As indicated in the inset pictures, three regimes are observed over the range of concentrations studied. From the Cassie-Baxter state below $C_p \approx 0.7$ mM to a dynamic regime in which CO_2 progressively invades the hydrophobic texture between C_p and C_l, the critical concentration for levitation. Above $C_l \approx 7$ mM, stable levitation is achieved, leading to a steady increase in initial levitation time. The dashed line is obtained by fitting measurements with a diffusion-based scaling that gives $\tau \propto (C_0 - C_l)^{2/3}$ (see section S8). (**B**) Direct interferometric measurement of initial gas film thickness h_0 as a function of the initial concentration C_0 of dissolved $CO_{2(aq)}$. Above $C_l \approx 7$ mM, in the levitating regime, the initial film thickness increases from 0.5 to 3 μm when $C_0 \approx 170$ mM.

dissolved $CO_{2(aq)}$ concentration (C_0) as determined by pH measurements. As noted above, no levitation is observed below a critical concentration of $CO_{2(aq)}$ denoted as C_l, an analog of the critical Leidenfrost temperature T_l. The thickness of the initial gas layer is measured above C_l and shows a monotonic increase with the initial concentration C_0. In the levitating regime (above C_l), the initial thickness of the insulating film rises from around 500 nm at $C_0 \approx 30$ mM to more than 3 μm when $C_0 \approx 170$ mM. The maximum value of the thickness measured here is almost one order of magnitude lower than in the case of Leidenfrost drops, where vapor thicknesses typically reach several tens of microns (*27*).

However, the values of the levitation time τ compare well to typical lifetimes of millimetric Leidenfrost drops (*27*) where the levitation is set by the evaporation of the entire volatile drop, although, here, only a much smaller mass (i.e., just the CO_2 dissolved in water) is released during the levitation process. A simple model can

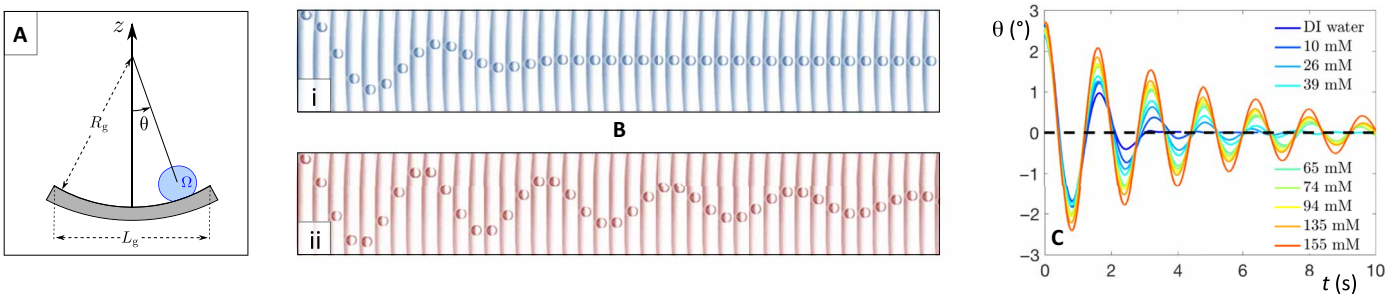

Fig. 4. Low-friction dynamics of fizzy levitating drops. (**A**) Sketch (not to scale) of a groove of constant radius of curvature $R_g = 635$ mm and of length $L_g = 65$ mm. The drop is released from the rim at one end of the groove, and its position is tracked by its angular position θ. (**B**) Sequence of top view images (time step of 20 ms) of the groove with 80-μl drops of, respectively, DI water (in blue) and carbonated water of initial concentration $C_0 = 168$ mM (in red). Starting from the rim of the groove, the drop oscillates around its equilibrium position (in the middle of the trough). After only two periods, the DI water drop arrests because of pinning on the substrate, whereas the carbonated water continues to oscillate after five complete periods. (**C**) Angular position θ of a 80-μl water drop oscillating in the groove as a function of time t for various initial concentrations of $CO_{2(aq)}$ ($0 \leq C_0 \leq 155$ mM). The period of the oscillations remains unchanged, but the damping coefficient changes, indicating a reduced friction in the case of levitating drops.

provide understanding of this apparent contradiction. The thin gas layer is pressurized by the drop (either because of its weight $\Delta P \sim \rho g H$ or the Laplace pressure $\Delta P \sim \gamma/R$), leading to a radial Poiseuille flow in the underlying gas film with velocity field $U(r, z)$, similar to classical laws in Leidenfrost regime (*6*, *27*). By assuming a uniform thickness for simplicity, a lubrication approximation allows us to solve analytically for this incompressible vapor flow, and we determine an average velocity that scales as $\overline{U} \sim \Delta P h^2/\eta_g r_c$ with η_g as the viscosity of $CO_{2(g)}$ and r_c as the size of the drop base. A mass balance in the vapor layer states that the release rate $\dot{m}$ scales as $\dot{m} \sim \rho_g r_c h \overline{U}$ with ρ_g as the density of $CO_{2(g)}$. Combining these two equations, we can deduce the scaling $\dot{m} \propto h^3$. For a carbonated water drop, the available fuel driving fizzy levitation is limited by the molar quantity of $CO_{2(aq)}$ dissolved in volume Ω [i.e., $(\Omega C_0) \approx 4$ μmol for a 40-μl carbonated droplet with an initial concentration of $C_0 \approx 0.1$ M]. This value is lower by three orders of magnitude than that for a classical Leidenfrost drop in which the whole liquid phase evaporates ($\Omega\rho_l/M_{H2O} \sim 2$ mmol for a 40-μl drop with $M_{H2O} = 18$ g/mol). The similar values of levitation time scales in both phenomena thus suggest a gas release rate $\dot{m}$ that is three orders of magnitude lower in the case of a fizzy droplet. While Leidenfrost drops experience rapid vapor flow in the gas cushion dominated by convection in the vapor cushion (*27*), the slow CO_2 release rate around a levitating carbonated drop is controlled by diffusion in a mass boundary layer (see section S8). In consequence, as $\dot{m} \propto h^3$, the thickness of the gas cushion adapts and decreases by one order of magnitude in good agreement with the measurements in Fig. 3B.

Applications of fizzy levitation

In Fig. 4, we investigate the dynamics of these levitating objects. Because the gas cushion insulates the drop from the underlying textured substrate, sliding friction is markedly reduced. In Fig. 4B, a drop is released at the rim of a superhydrophobic-coated trough of constant curvature (see Materials and Methods) sketched in Fig. 4A. While the DI water drop oscillates only twice about the center of the groove (Fig. 4B, i), carbonated drops at higher $CO_{2(aq)}$ concentrations ($C_0 \gg C_l$) exhibit a larger number of damped oscillations, demonstrating substantially enhanced mobility due to smaller friction (*28*). By tracking the drops, we extract the time-dependent position θ(t) of the drop in Fig. 4C. We observe a damped harmonic oscillator behavior for different initial concentrations of CO_2. The period of oscillations is not affected by C_0 with a constant value about 1.6 s, a value in good agreement with the pendulum analogy ($\omega = \sqrt{g/R_g} \approx 4$ rad/s; see section S9). However, the damping coefficient varies markedly between low CO_2 concentration (blue symbols) and larger concentrations (red symbols). The number of oscillations increases with the initial CO_2 concentration, indicating that the low value of the friction coefficient for a water drop on a superhydrophobic coating becomes even smaller with carbonated water; the released CO_2 vapor insulates the drop from discrete pinning events on the randomly textured substrate. By considering viscous dissipation in the gas cushion during the levitating regime, we can capture the damped periodic oscillations in the measured position θ(t) and extract values for the dynamic gas film thickness (typically a few microns), which are in good agreement with the interferometric measurements shown in Fig. 3B (see section S9). The levitation of fizzy fluids thus results in dynamic properties analogous to Leidenfrost droplets in terms of reduction of sliding friction.

Thermally levitating Leidenfrost drops have also been shown to self-propel on substrates featuring millimetric-scale machined textures (*9*). Volatile drops placed on hot ratchet substrates propel in a given direction due to the viscous entrainment of the asymmetric vapor-insulating layer that imposes a net lateral force on the drop. We machined a brass ratchet with asymmetric teeth of pitch λ = 1.5 mm and height ε = 0.3 mm. When a 300-μl carbonated drop ($C_0 = 97$ mM) is deposited on the ratchet, we observe a redirection of the drop in the direction of the ratchet teeth (movie S6). The drop self-propels (from left to right) with a steady terminal velocity of around 15 mm/s, a value 10 times smaller than the traditional Leidenfrost case (*10*) but yet comparable to the "cold" Leidenfrost regime recently observed on warm superhydrophobic substrates (*29*). This decrease in the propulsion velocity arises from the reduced thickness of the gas layer in our room temperature regime and the concomitant increase in the vapor phase friction.

We can also generalize this vapor-mediated technique to incorporate other "chemically active" drops able to generate their own levitation. In this paper, we have focused on the case of carbon dioxide dissolved in water at room temperature. We can easily dissolve other gases of even higher solubility. We can also use chemical

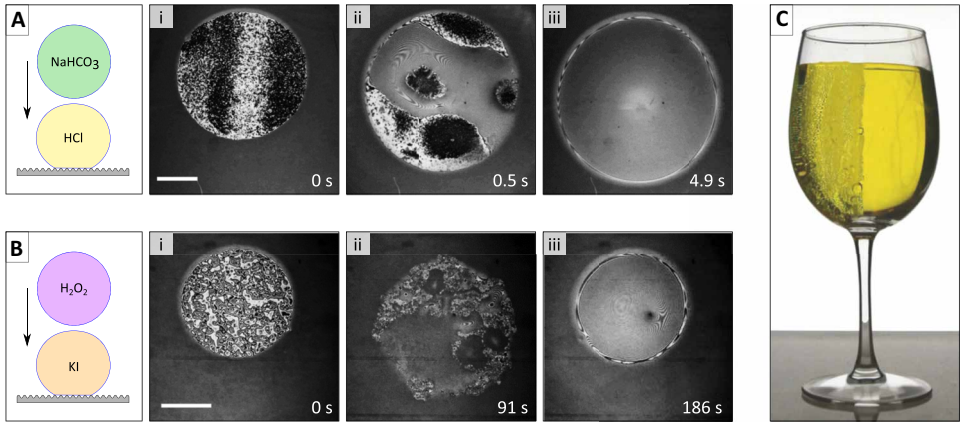

Fig. 5. Generality of fizzy levitating drops. (**A**) A 20-μl drop of sodium bicarbonate (0.5 M) is deposited on the top of a droplet of hydrochloric acid (20 μl, 0.5 M) initially sitting in the Cassie-Baxter state on a Glaco-coated glass slide (i). The generation of $CO_{2(g)}$ leads to the formation of bubbles (ii) and, ultimately, to the levitation of the entire drop (iii). (**B**) When mixing a drop of hydrogen peroxide (10 μl, $[H_2O_2] = 9.8$ M) into a drop of an aqueous solution of potassium iodide (10 μl, [KI] = 0.18 M), $O_{2(g)}$ is generated and levitation is again eventually achieved. Scale bars, 0.5 mm. (**C**) Carbonated water ($C_0 = 168$ mM) in a wine glass treated with Glaco coating on one half (right) and untreated on the other half (left). Similar to the Leidenfrost effect, we observe the difference between "nucleate boiling" on the hydrophilic surface (left) and film boiling on the superhydrophobic glass (right). Photo credit: D. Panchanathan and P. Bourrianne, MIT.

reactions to generate $CO_{2(g)}$. In Fig. 5A (i), a 20-μl drop of an aqueous solution of HCl (0.5 M) sits on a Glaco-coated glass slide. Interferometry images of the base of the drop indicate that the liquid is partially repelled and initially establishes a Cassie-Baxter regime. When a second 20-μl drop of an aqueous solution of sodium bicarbonate $NaHCO_3$ (0.5 M) is deposited on top, both liquids mix and react through the acid-mediated decomposition of sodium bicarbonate $NaHCO_{3(aq)} + HCl_{(aq)} \rightarrow NaCl_{(aq)} + H_2O_{(l)} + CO_{2(g)}$ (*30*). This gas is then released and leads to the formation of bubbles that spread across the superhydrophobic coating (Fig. 5A, ii) and eventually merge, leading to levitation (Fig. 5A, iii, and movie S7). Experiments show that this self-levitation of chemically reactive liquids also requires a large enough rate of release of $CO_{2(g)}$ vapor and a superhydrophobic substrate (section S14). Moreover, other gases, such as O_2 in Fig. 5B, can also provide levitation. When a 10-μl drop of an aqueous solution of potassium iodide (at an initial concentration of [KI] = 0.18 M) resides on the superhydrophobic transparent surface in Fig. 5B (i), it sits on the top of the texture exhibiting a Cassie-Baxter state. In Fig. 5B (ii), a 10-μl drop of hydrogen peroxide H_2O_2 (9.8 M) is added to the first drop. As potassium iodide catalyzes the decomposition of hydrogen peroxide (*31*, *32*), a rapid reaction takes place that generates $O_{2(g)}$. This gas also eventually leads to complete droplet levitation as depicted in Fig. 5B (iii). It is evident that levitation can be generated from a wide variety of liquids that are able to support their own weight, either from supersaturated gas emission situations or chemical reactions. It is remarkable to notice that chemically reactive liquids can also provide an example of a marked wetting transition in which the liquid droplet that is initially wetting the water-repellent substrate in a Cassie-Baxter state jumps into a state of levitation.

By dissolving $CO_{2(aq)}$ in water, we have demonstrated the levitation of carbonated water droplets by taking advantage of sustained gas release from the supersaturated liquid. These hovering objects have an extremely low friction with remarkable mobility and the ability to self-propel on a thin dynamic gas film. The dynamic properties of these sustained gas films might also be extended to larger volumes of liquid (as shown in Fig. 5C and movie S8) where localized nucleation of $CO_{2(g)}$ bubbles on a hydrophilic glass surface can be eliminated by establishing a contiguous plastron of released CO_2, which is of possible interest in beverage packaging.

In contrast to conventional Leidenfrost, fizzy levitation occurs at ambient temperature in a regime not affected by droplet evaporation, an observation of obvious practical interest. Its smooth and continuous transition (with no nucleate boiling) enables systematic studies that can provide a better fundamental understanding of Leidenfrost transitions. We have also demonstrated that room temperature levitation can be achieved using other kinds of active liquids such as chemically reacting droplets that are able to generate and release gas. Last, this levitation approach can be also broadly applied to nonvolatile liquids such as oils and other nonaqueous liquids containing dissolved gases by using superomniphobic surfaces (*33*–*35*).

MATERIALS AND METHODS

Superhydrophobic coating

Our Glaco coating is prepared with a colloidal solution, Glaco Mirror Coat Zero purchased from Soft99 Co. (Japan). The deposited solid films drawn out of the Glaco dispersions are postbaked at 250°C for 30 min, a process repeated three times to provide a homogeneous coating with minimal pinning points (section S1). Advancing and receding angles of water at ambient temperature are, respectively, $\theta_a = 169° \pm 2°$ and $\theta_r = 165° \pm 2°$, which leads to a very low contact angle hysteresis $\Delta\cos\theta = \cos\theta_r - \cos\theta_a = 10^{-2}$.

Concentration of $CO_{2(aq)}$

Carbonated water was prepared by pressurizing gaseous carbon dioxide into DI water at ambient temperature. Commercially available polyethylene terephthalate bottles (purchased from Poland Spring) were closed with a carbonation cap (Ferroday) and connected to a gas line (CMBecker), which delivers carbon dioxide from a CO_2 tank (Airgas) under constant CO_2 pressure delivered by a CO_2

pressure regulator (Airgas/Harris). The initial concentration C_0 of $CO_{2(aq)}$ dissolved in water was estimated by immersing a micro pH electrode (Thermo Scientific Orion) as described in section S2. The volume of the drops was also carefully calibrated (section S10).

Interferomicroscopy setup

The base of drops was imaged using a 4× objective mounted on an inverted microscope (Nikon Eclipse TE2000-U) connected to a digital camera (GH5 Lumix). Illumination was provided via a filter cube consisting of a semireflective mirror, a filter ($\lambda = 542 \pm 15$ nm) for the incident light, and no filter for the emitted/reflected light. The drops were kept stationary in the field of view of the microscope by trapping them with superhydrophobic annular rings (see section S12).

Measurement of the gas thickness

The measurement of the minimum gas thickness h at the rim was obtained after imaging the edge of the drop base with a 20× objective mounted on the inverted microscope and connected to a high-speed camera (Phantom Miro 320S). Successive interference fringes were counted to back-calculate the evolution in the minimum gas film thickness $h(t)$ at the edge of the levitating drop (movies S4 and S5). The initial thickness h_0 was reported after the stabilization of the interface, while the reading remains roughly constant for a few seconds.

Trough

The trough (of radius of curvature $R_g = 635$ mm and of length $L_g = 65$ mm, i.e., a slope < 6°) sketched in Fig. 4A was machined in aluminum. Experiments were carried out by capturing top views with a high-speed camera (Phantom Miro 320S). To prevent any lateral motion of the drop, we added a secondary curvature in the orthogonal direction of the motion.

SUPPLEMENTARY MATERIALS

Supplementary material for this article is available at http://advances.sciencemag.org/cgi/content/full/7/28/eabf0888/DC1

REFERENCES AND NOTES

1. Y. Couder, E. Fort, C.-H. Gautier, A. Boudaoud, From bouncing to floating: Noncoalescence of drops on a fluid bath. *Phys. Rev. Lett.* **94**, 177801 (2005).
2. H. Lhuissier, Y. Tagawa, T. Tran, C. Sun, Levitation of a drop over a moving surface. *J. Fluid Mech.* **733**, (2013).
3. D. Foresti, M. Nabavi, M. Klingauf, A. Ferrari, D. Poulikakos, Acoustophoretic contactless transport and handling of matter in air. *Proc. Natl. Acad. Sci. U.S.A.* **110**, 12549–12554 (2013).
4. M. A. Weilert, D. L. Whitaker, H. J. Maris, G. M. Seidel, Magnetic levitation and noncoalescence of liquid helium. *Phys. Rev. Lett.* **77**, 4840–4843 (1996).
5. J. G. Leidenfrost, De Aquae Communis Nonnullis Qualitatibus Tractatus (Ovenius, Duisburg, 1756).
6. D. Quéré, Leidenfrost dynamics. *Annu. Rev. Fluid Mech.* **45**, 197–215 (2013).
7. I. U. Vakarelski, J. O. Marston, D. Y. C. Chan, S. T. Thoroddsen, Drag reduction by Leidenfrost vapor layers. *Phys. Rev. Lett.* **106**, 214501 (2011).
8. D. Saranadhi, D. Chen, J. A. Kleingartner, S. Srinivasan, R. E. Cohen, G. H. McKinley, Sustained drag reduction in a turbulent flow using a low-temperature Leidenfrost surface. *Sci. Adv.* **2**, e1600686 (2016).
9. H. Linke, B. J. Alemán, L. D. Melling, M. J. Taormina, M. J. Francis, C. C. Dow-Hygelund, V. Narayanan, R. P. Taylor, A. Stout, Self-propelled Leidenfrost droplets. *Phys. Rev. Lett.* **96**, 154502 (2006).
10. G. Lagubeau, M. Le Merrer, C. Clanet, D. Quéré, Leidenfrost on a ratchet. *Nat. Phys.* **7**, 395–398 (2011).
11. G. G. Wells, R. Ledesma-Aguilar, G. McHale, K. Sefiane, A sublimation heat engine. *Nat. Commun.* **6**, 6390 (2015).
12. A. Bouillant, T. Mouterde, P. Bourrianne, A. Lagarde, C. Clanet, D. Quéré, Leidenfrost wheels. *Nat. Phys.* **14**, 1188–1192 (2018).
13. B. S. Gottfried, C. J. Lee, K. J. Bell, The leidenfrost phenomenon: Film boiling of liquid droplets on a flat plate. *Int. J. Heat Mass Transf.* **9**, 1167–1188 (1966).
14. J. D. Bernardin, I. Mudawar, The Leidenfrost point: Experimental study and assessment of existing models. *J. Heat Transfer* **121**, 894–903 (1999).
15. I. U. Vakarelski, N. A. Patankar, J. O. Marston, D. Y. C. Chan, S. T. Thoroddsen, Stabilization of Leidenfrost vapour layer by textured superhydrophobic surfaces. *Nature* **489**, 274–277 (2012).
16. L. Maquet, B. Sobac, B. Darbois-Texier, A. Duchesne, M. Brandenbourger, A. Rednikov, P. Colinet, S. Dorbolo, Leidenfrost drops on a heated liquid pool. *Phys. Rev. Fluids.* **1**, 053902 (2016).
17. P. Bourrianne, C. Lv, D. Quéré, The cold Leidenfrost regime. *Sci. Adv.* **5**, eaaw0304 (2019).
18. A. B. D. Cassie, S. Baxter, Wettability of porous surfaces. *Trans. Faraday Soc.* **40**, 546 (1944).
19. D. Quéré, Wetting and roughness. *Annu. Rev. Mat. Res.* **38**, 71–99 (2008).
20. R. N. Wenzel, Surface roughness and contact angle. *J. Phys. Colloid Chem.* **53**, 1466–1467 (1949).
21. A. Lafuma, D. Quéré, Superhydrophobic states. *Nat. Mater.* **2**, 457–460 (2003).
22. J. C. Burton, A. L. Sharpe, R. C. A. van der Veen, A. Franco, S. R. Nagel, Geometry of the vapor layer under a Leidenfrost drop. *Phys. Rev. Lett.* **109**, 074301 (2012).
23. J. H. Snoeijer, P. Brunet, J. Eggers, Maximum size of drops levitated by an air cushion. *Phys. Rev. E* **79**, 036307 (2009).
24. R. Sander, Compilation of Henry's law constants (version 4.0) for water as solvent. *Atmos. Chem. Phys.* **15**, 4399–4981 (2015).
25. T. Takahashi, Carbon dioxide in the atmosphere and in Atlantic Ocean water. *J. Geophys. Res.* **66**, 477 (1961).
26. H. de Maleprade, C. Clanet, D. Quéré, Spreading of bubbles after contacting the lower side of an aerophilic slide immersed in water. *Phys. Rev. Lett.* **117**, 094501 (2016).
27. A.-L. Biance, C. Clanet, D. Quéré, Leidenfrost drops. *Phys. Fluids* **15**, 1632 (2003).
28. J. V. I. Timonen, M. Latikka, O. Ikkala, R. H. A. Ras, Free-decay and resonant methods for investigating the fundamental limit of superhydrophobicity. *Nat. Commun.* **4**, 2398 (2013).
29. G. Dupeux, P. Bourrianne, Q. Magdelaine, C. Clanet, D. Quéré, Propulsion on a superhydrophobic ratchet. *Sci. Rep.* **4**, 5280 (2015).
30. F. J. W. Roughton, The kinetics and rapid thermochemistry of carbonic acid. *J. Am. Chem. Soc.* **63**, 2930–2934 (1941).
31. H. A. Liebhafsky, The catalytic decomposition of Hydrogen peroxide by the iodine-iodide couple at 25°. *J. Am. Chem. Soc.* **54**, 1792–1806 (1932).
32. D. Panchanathan, A. Rajappan, K. K. Varanasi, G. H. McKinley, Plastron regeneration on submerged superhydrophobic surfaces using in situ gas generation by chemical reaction. *ACS Appl. Mater. Interfaces* **10**, 33684–33692 (2018).
33. A. Tuteja, W. Choi, M. Ma, J. M. Mabry, S. A. Mazzella, G. C. Rutledge, G. H. McKinley, R. E. Cohen, Designing superoleophobic surfaces. *Science* **318**, 1618–1622 (2007).
34. T. Liu, C.-J. Kim, Turning a surface superrepellent even to completely wetting liquids. *Science* **346**, 1096–1100 (2014).
35. S. Pan, R. Guo, M. Björnmalm, J. J. Richardson, L. Li, C. Peng, N. Bertleff-Zieschang, W. Xu, J. Jiang, F. Caruso, Coatings super-repellent to ultralow surface tension liquids. *Nat. Mater.* **17**, 1040–1047 (2018).
36. T. Mouterde, G. Lehoucq, S. Xavier, A. Checco, C. T. Black, A. Rahman, T. Midavaine, C. Clanet, D. Quéré, Antifogging abilities of model nanotextures. *Nat. Mater.* **16**, 658–663 (2017).
37. D. Panchanathan, thesis, Deparment of Mechanical Engineering, MIT (2018);dspace.mit.edu/handle/1721.1/120260.
38. C. E. Housecroft, A. G. Sharpe, *Inorganic Chemistry* (Pearson Education Ltd., ed. 4, 2012).
39. S. C. Wong, Elevated atmospheric partial pressure of CO_2 and plant growth: I. Interactions of nitrogen nutrition and photosynthetic capacity in C_3 and C_4 plants. *Oecologia* **44**, 68–74 (1979).
40. T. Mouterde, P. S. Raux, C. Clanet, D. Quéré, Superhydrophobic frictions. *Proc. Natl. Acad. Sci.* **116**, 8220–8223 (2019).
41. D. Panchanathan, P. Bourrianne, K. K. Varanasi, G. H. McKinley, Reduced adhesion of sparkling water droplets. *Phys. Rev. Fluids* **4**, 100505 (2019).
42. J. de Ruiter, R. Lagraauw, D. van den Ende, F. Mugele, Wettability-independent bouncing on flat surfaces mediated by thin air films. *Nat. Phys.* **11**, 48–53 (2015).

Acknowledgments: We thank A. Schwartzman (NanoLab, MIT) for assistance with atomic force microscopy imaging, the MIT Central Machine Shop for manufacturing the aluminum trough, and A. Rajappan for assistance with videography in movie S8. We also thank D. Quéré for insightful discussions. **Funding:** D.P. was supported in part by funding provided to K.K.V. and G.H.M. from the Center for Clean Water and Clean Energy (CCWCE) at MIT and at King Fahd University of Petroleum and Minerals (KFUPM). P.B. was supported by a gift to G.H.M. from Procter & Gamble. **Author contributions:** D.P., P.B., K.K.V., and G.H.M conceived the

project. D.P. and P.B. designed and analyzed the experiments. D.P., P.B., P.N., and A.C. performed the experiments. D.P., P.B., and G.H.M. wrote the manuscript with inputs from K.K.V. D.P. and P.B. have equally contributed to this work. **Competing interests:** The authors declare that they have no competing interests. **Data and materials availability:** All data needed to evaluate the conclusions in the paper are present in the paper and/or the Supplementary Materials. Additional data related to this paper may be requested from the authors.

Submitted 2 October 2020
Accepted 26 May 2021
Published 7 July 2021
10.1126/sciadv.abf0888

Citation: D. Panchanathan, P. Bourrianne, P. Nicollier, A. Chottratanapituk, K. K. Varanasi, G. H. McKinley, Levitation of fizzy drops. *Sci. Adv.* **7**, eabf0888 (2021).

Science Advances

Levitation of fizzy drops

Divya Panchanathan, Philippe Bourrianne, Philippe Nicollier, Abhijatmedhi Chottratanapituk, Kripa K. Varanasi and Gareth H. McKinley

Sci Adv **7** (28), eabf0888.
DOI: 10.1126/sciadv.abf0888